The Influence of Alloying Elements on Impurity Induced Grain Boundary Embrittlement

D. Y. LEE, E. V. BARRERA, J. P. STARK, and H. L. MARCUS

A nonequilibrium thermodynamic model which describes the effect of solute grain boundary segregation on grain boundary cohesion was extended to Fe ternary systems. The extended model directly and simply predicts the effect of alloying elements on impurity-induced grain boundary embrittlement. According to the extended model, Mo, W, and Zr strongly reduce, Ni, Ti, and V slightly reduce, and Cr and Mn enhance impurity-induced grain boundary embrittlement in an Fe ternary system. For the evaluation of the extended model, Fe-P, Fe-P-Mn, Fe-P-Mo, and Fe-P-W alloys were studied by Auger electron spectroscopy, scanning electron microscopy, 4-point slow bend tests, and tension tests. The experimental results show that for a given amount of P grain boundary segregation the grain boundary strength increases with increasing Mo or W grain boundary segregation and decreases with increasing Mn grain boundary segregation. These experimental results showing the remedial effect of Mo or W and the embrittling effect of Mn on P-induced grain boundary embrittlement are consistent with the predicted results from the extended model. The nonequilibrium model is also used to evaluate impurity-induced interfacial embrittlement in continuous fiber metal matrix composite materials.

I. INTRODUCTION

RECENTLY, Stark and Marcus[1] have developed a thermodynamic model which describes the effect of impurity (I) grain boundary segregation on the grain boundary cohesive energy. The development of the model was based upon a detailed nonequilibrium thermodynamic analysis of the grain boundary segregation process. This nonequilibrium model directly and simply provides a numerical estimate of the grain boundary cohesive energy change associated with impurity grain boundary segregation. However, it has been recognized that understanding the role of alloying elements (A) of the transition series is of great importance to predict and control grain boundary embrittlement in Fe alloys since the complex grain boundary embrittlement behavior is often encountered with the presence of alloying elements in Fe alloys. The effect of alloying elements on grain boundary embrittlement can be classified into the direct effect and the indirect effect. The indirect effect arises from the grain boundary cohesive energy change induced by the change in impurity grain boundary segregation due to the existence of the I-A interaction in Fe alloys. The I-A interaction and its effect on impurity grain boundary segregation has been rationalized by the Guttmann model.[2] However, the direct effect of alloying elements which arises from the grain boundary cohesive energy change induced by their own grain boundary segregation has as yet to be considered.

The main purpose of this study is to investigate the combined direct and indirect effect of alloying elements on impurity-induced grain boundary embrittlement. Therefore, the nonequilibrium model will be extended to Fe-I-A ternary systems. This will be followed by the experimental study on high purity Fe-P, Fe-P-Mn, Fe-P-Mo, and Fe-P-W alloys for the evaluation of the extended model. In order to determine grain boundary strength, the method recently developed by Kameda *et al.*[3,4] will be adopted.

D. Y. LEE is Senior Research Engineer with General Dynamics Corporation, P. O. Box 748, Fort Worth, TX 76101. E. V. BARRERA, Graduate Research Assistant, J. P. STARK, Professor, and H. L. MARCUS, H. L. Kent, Jr. Professor, are all with the Department of Mechanical Engineering, The University of Texas, Austin, TX 78712.

Manuscript submitted September 13, 1983.

II. THE EXTENDED NONEQUILIBRIUM MODEL

It is assumed in the development of the nonequilibrium model that the grain boundary (GB) region consists of the boundary (B) and boundary matrix interface (BM) regions as shown in Figure 1. Also, the thicknesses of these B and BM regions are assumed to be atomic in nature. The development of the extended model is presented in detail in Appendix B. The final result of the extended model can be expressed as:

$$\begin{aligned}\delta H^{GB} &= \delta H^{B} + \delta H^{BM} \\ &= \delta H^{B}_{*} + \delta H^{BM}_{*} - ({}^{m}\overline{H}^{M}_{I} + \underline{H}^{M}_{I} - \underline{H}^{M}_{\mathrm{Fe}})\,\delta N^{M}_{I} \\ &\quad - ({}^{m}\overline{H}^{M}_{A} + \underline{H}^{M}_{A} - \underline{H}^{M}_{\mathrm{Fe}})\,\delta N^{M}_{A} \qquad [1]\end{aligned}$$

Where δH^{GB}, δH^{B}, and δH^{BM} are enthalpy changes in GB, B, and BM during grain boundary segregation, respectively, ${}^{m}\overline{H}^{M}_{I}$ and ${}^{m}\overline{H}^{M}_{A}$ are the partial molar mixing enthalpies of an impurity I and an alloying element A in the matrix (M), respectively, $\underline{H}^{M}_{I}$, $\underline{H}^{M}_{A}$, and $\underline{H}^{M}_{\mathrm{Fe}}$ are the molar enthalpies of pure I, A, and Fe, respectively, and δN^{M}_{I} and δN^{M}_{A} are the changes in the number of moles of I and A in M, respectively. The terms δH^{B}_{*} and δH^{BM}_{*} in Eq. [1] are the enthalpy changes in B and BM, respectively, when B and BM transform from their initial high grain boundary energy state to their final low grain boundary energy state. This transformation is equivalent to the system undergoing grain boundary segregation as an attempt to obliterate the high grain boundary energy. A better understanding of these terms may be obtained from the details of the nonequilibrium model development presented in Reference 1.

Matrix (M)	
Boundary Matrix Interface (BM)	s^{BM}
Boundary (B)	s^{B}
Boundary Matrix Interface (BM)	s^{BM}
Matrix (M)	

Fig. 1 — Model of grain boundary region [1].

Since the "pV" terms associated with enthalpy are generally negligible in condensed phases, the enthalpy change in the grain boundary during grain boundary segregation is virtually equal to the change in the grain boundary cohesive energy because it reflects the change in the depth of the energy-well holding the atoms together. Then, it can be noted from Eq. [1] that the grain boundary cohesive energy change associated with grain boundary segregation is given as a function of the partial molar mixing enthalpies of I and A, the molar enthalpies of I, A, and Fe, and the changes in the number of moles of I and A in M. The partial molar enthalpies and the molar enthalpies can be obtained from the published thermodynamical data, and the changes in the number of moles of I and A can be determined from grain boundary chemistry analysis. Thus, a numerical estimate of the grain boundary cohesive energy change associated with grain boundary segregation can be made by using Eq. [1] with a proper approximation of the terms δH_*^B and δH_*^{BM}.

Stark and Marcus[1] have shown that the sum of the two terms, $\delta H_*^B + \delta H_*^{BM}$, is energetically equivalent to the energy required for the removal of the grain boundary at the initial grain boundary composition (*i.e.*, $\delta H_*^B + \delta H_*^{BM} \simeq -22$ kJ/mole). The molar enthalpies are substituted by the negative values of the published molar sublimation enthalpies.[5] Finally, the partial molar mixing enthalpies ($^m\overline{H}_I^M$ and $^m\overline{H}_A^M$) are determined from the details of the Fe-I or Fe-A binary phase diagram[6] by using a method discussed by Swalin.[7] Here, impurities include the well-known embrittling elements in Fe alloys such as As, P, Pb, S, Sb, Se, Sn, and Te, and alloying elements include the commonly found metallic additions of transition series such as Cr, Mn, Mo, Ni, Ti, V, W, and Zr. Table I lists the molar enthalpies and partial molar mixing enthalpies of the above impurities and alloying elements. As shown in Table I, the contribution of the partial molar mixing enthalpies to the estimation of the grain boundary cohesive energy change is quite small for most impurities and alloying elements. Therefore, this term will be ignored for the element whose partial molar mixing enthalpy could not be determined.

Table II shows the estimated value of the grain boundary cohesive energy change when a monolayer of either an impurity or an alloying element is present at the grain boundary in an Fe-I or an Fe-A binary system. It can be seen from Table II that all the impurities which have been known as grain boundary embrittlers reduce the grain boundary cohesive energy. Even the order of the embrittling potencies (P^E) of P, Sb, and Sn is perfectly consistent with that found in experiments; the P^E of P, Sb, and Sn have been experimentally found to have the order of $P^E(\text{Sb}) > P^E(\text{Sn}) > P^E(\text{P})$.[9] However, the predicted P^E for S appears to be somewhat less than expected.

Table I. Molar Enthalpies and Partial Molar Mixing Enthalpies of Impurities and Alloying Elements (Unit: kJ/mole)

I	H_I^M	$^m\overline{H}_I^M$	A	H_A^M	$^m\overline{H}_A^M$
As	289	5	Cr	397	*
P [1]	334	13	Mn	279	23
Pb	196	1	Mo [8]	659	31
S [1]	276	67	Ni	427	14
Sb	259	9	Ti	472	5
Se	207	*	V	515	*
Sn	301	7	W	837	9
Te	192	*	Zr	611	163

Table II. Grain Boundary Cohesive Energy Change with a Monolayer Grain Boundary Segregation of I or A in Fe-I and Fe-A Binary Systems (kJ/Monolayer)

Fe-I System		Fe-A System	
I	δH^{GB}	A	δH^{GB}
As	−144	Cr	− 41
P	− 91	Mn	−136
Pb	−242	Mo	+252
S	− 95	Ni	+ 3
Sb	−170	Ti	+ 39
Se	−231	V	+ 77
Sn	−130	W	+408
Te	−246	Zr	+336

In the case of alloying elements, most of them are beneficial to the grain boundary cohesive energy except Cr and Mn. In particular, Mn exhibits a fairly high embrittling potency (*i.e.*, even higher than P, S, and Sn for a given amount of grain boundary segregation). Of course, the grain boundary segregation enrichment ratio of Mn is much less than those of impurities. However, it is of interest to note that Schulz and McMahon[10] have experimentally found that in the absence of impurities, Mn itself causes grain boundary embrittlement in an Fe-0.7 Mn-0.4C system.

For Fe-I-A ternary systems, Figure 2 shows the variation of the grain boundary cohesive energy change with the molar fractional monolayer of alloying elements at the grain boundary where 0.5 monolayer of P is already present. From Figure 2 the direct effect of alloying elements on P-induced grain boundary embrittlement can be observed. By their direct effect, Mo, W, and Zr strongly reduce, Ni, Ti, and V slightly reduce, and Cr and Mn enhance P-induced grain boundary embrittlement in Fe alloys. These predicted results are consistent with the published experimental results showing the remedial effect of Mo[10,11,12] and Ti[13,14] and the embrittling effect of Cr[11,15-17] and Mn[18,19,20] on impurity-induced grain boundary embrittlement.

It is also of great interest to note that Schulz and McMahon[10] have experimentally found that Mo reduces Mn-induced grain boundary embrittlement in an Fe-0.7 Mn-0.6 Mo-0.4C system. The remedial effect of alloying elements has been attributed only to the indirect effect arising from the strong attractive I-A interaction which reduces impurity grain boundary segregation by precipitating the impurity in the matrix. However, the above interesting Mn-Mo behavior can be explained by the direct effect of Mn and Mo on the grain boundary cohesive energy. When both Mn and Mo simultaneously segregate to the grain boundary, Mn embrittles the grain boundary by its embrittling direct effect, while Mo improves the grain boundary cohesive energy by its remedial effect, thereby relieving Mn-induced grain boundary embrittlement.

Here, the effects of alloying elements were considered only on P-induced grain boundary embrittlement in Fe-I-A alloys. By using Eq. [1] the similar diagrams to Figure 2 can be generated for other embrittling elements in Fe-I-A alloys as well as non-Fe base alloys. Also, the nonequilibrium model can be applied to the interfacial embrittlement problems associated with impurity interfacial segregation in continuous fiber metal matrix composite materials as presented in Appendix C.

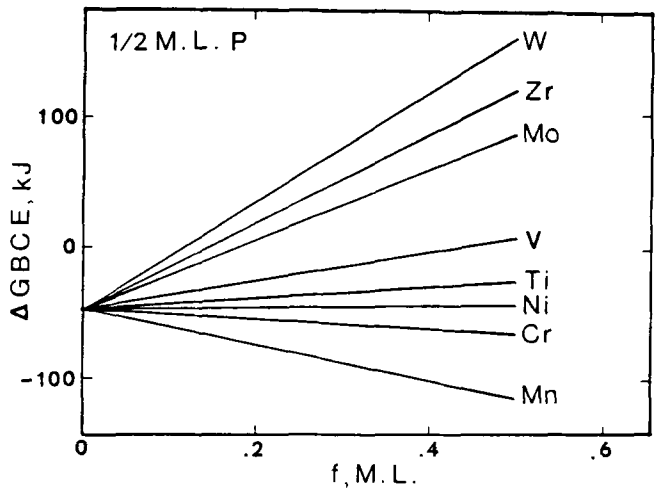

Fig. 2—The variation of grain boundary cohesive energy change with the fraction of a monolayer of grain boundary segregation of alloying elements with ½ monolayer P grain boundary segregation.

Recently, Seah[21] has proposed a simple pair bonding theory describing the grain boundary fracture energy change associated with solute grain boundary segregation in a binary system. Seah's result can be written as:

$$\Delta\gamma^{GB} = (Z^{GB}/Z^{M})X_2^{GB}(H_1^* - H_2^*) \qquad [2]$$

where $\Delta\gamma^{GB}$ is the grain boundary fracture energy change associated with solute grain boundary segregation, Z^{GB} and Z^{M} are the coordination numbers of the atom in the grain boundary and the matrix, respectively, X_2^{GB} is the molar fractional monolayer of the solute 2 in the grain boundary, and H_1^* and H_2^* are the sublimation enthalpies per unit area of pure solvent 1 and pure solute 2, respectively. Here, the grain boundary fracture energy change, that is equivalent to the grain boundary cohesive energy change associated with solute grain boundary segregation, is directly related to the difference between the sublimation enthalpies of solvent and solute. The approach of Seah's pair bonding theory is quite different from that of the extended nonequilibrium model. However, it can be noted from Eqs. [1] and [2] that these two different theories show basically the same result that the grain boundary cohesive energy change associated with grain boundary segregation is directly related to the difference between the sublimation enthalpies of solvent and solute.

By applying equilibrium thermodynamics to the energetics of brittle fracture, several investigators[22,23] have attempted to calculate the work of brittle grain boundary fracture. According to the above approaches the work of brittle grain boundary fracture is often stated by the expression $2\gamma^S - \gamma^{GB}$, where γ^S and γ^{GB} are the surface energy and the grain boundary energy, respectively. The implication is that γ^S and γ^{GB} are equilibrium thermodynamic values. However, McMahon *et al.*[24,25] have criticized these attempts since fracture is essentially an irreversible process.

Recently, Losch[26,27] and Briant and Messmer[28,29,30] have studied the chemical bonding aspects of grain boundary embrittlement. Their results have suggested that the grain boundary embrittling impurities draw charge from the neighboring metal-metal bonds, which hold the grain boundary together, to form strong impurity-metal bonds within the plane of the grain boundary. Thus, the metal-metal bonds across the grain boundary will be weakened, thereby leading to grain boundary embrittlement. The results[30] have also shown that P is more electronegative with respect to Cr and Mn than to Fe and more charge will be drawn from Cr and Mn onto P. Therefore, Cr and Mn exhibit an embrittling effect on *P*-induced grain boundary embrittlement. However, P is less electronegative with respect to Ni than to Fe. Consequently, Ni does not enhance *P*-induced grain boundary embrittlement. Even though the interactions between *I*, *A*, and Fe were not included in the extended nonequilibrium model, it can be noted that the predicted results on Cr, Mn, and Ni from the extended model are consistent with the above results.

III. EXPERIMENTAL PROCEDURES

The materials used in this study are high purity Fe-P, Fe-P-Mn, Fe-P-Mo, and Fe-P-W alloys prepared at the General Electric Research and Development Center in the form of hot rolled plates of 12.7 mm in thickness and 76.2 mm in width. The chemical compositions of these alloys were analyzed by Anderson & Associates, Houston, Texas and Chicago Spectro Service Laboratory, Chicago, Illinois. The analyzed chemical compositions of the alloys are shown in Table III.

The reasons for choosing these alloys are the following:

1. Among the well-known grain boundary embrittling impurities (*i.e.*, As, P, S, Sb, Sn, *etc.*), P is the most common impurity in commercial Fe alloys. Hence, the study on P grain boundary segregation and its effect on grain boundary embrittlement is of practical importance.
2. As discussed earlier, the extended model suggests the remedial effect of Mo and W and the embrittling effect of Mn on *P*-induced grain boundary embrittlement. Therefore, the P-doped Fe alloys that individually contain Mn, Mo, or W were selected in order to evaluate experimentally the extended model.
3. C often causes a complex situation in grain boundary embrittlement studies by segregating to grain boundaries in elemental form and/or by precipitating at grain boundaries in the form of carbides. Hence, the low C content Fe alloys as shown in Table III were chosen to avoid this complex situation.
4. Finally, the effect of alloying elements on impurity-induced grain boundary embrittlement may arise not only from the direct effect but also from the indirect effect. Therefore, for careful study on the indirect effect of Mn, Mo, and W, the level of P grain boundary segregation in the ternary Fe-P-Mn, Fe-P-Mo, and Fe-P-W alloys are to be compared to that in the binary Fe-P alloy.

For heat treatments the plates were cut into the rectangular blocks of 12.7 mm × 21.4 mm × 76.2 mm. As pointed out previously,[31,32] the mechanical-structural factors such as hardness, grain size, morphology of grain boundary, and type of microstructure are important variables controlling grain boundary embrittlement. Since the main purpose of this study is to investigate the effect of P, Mn, Mo, and W grain boundary segregation on the grain boundary strength, it would be desirable not to have variables of the mechanical-structural factors. Therefore, the first heat

Table III. The Chemical Compositions of Materials (Wt Pct)

Element	Fe-P		Fe-P-Mn		Fe-P-Mo		Fe-P-W	
	(a)	(b)	(a)	(b)	(a)	(b)	(a)	(b)
B	0.0003		<0.0001		0.002		0.001	
C	0.001	0.001	0.011	0.0080	0.008	0.0080	0.014	0.0090
P	0.1	0.057	0.1		0.1		0.1	
S	0.003	<0.005	0.004		0.003		0.005	
Si	0.008	0.01	0.005		0.068		0.015	
Al	<0.0006		<0.0006		0.02		<0.0006	
Co	<0.002		<0.002		<0.002		0.005	
Cr	0.004	0.01	0.018		0.005		0.011	
Cu	<0.0009	<0.01	<0.0009		<0.0009		<0.0009	
Mn	0.01	0.01	2.6		0.034		0.015	
Mo	0.004	<0.01	0.08		3.2		0.034	
Nb	<0.005		<0.005		<0.005		<0.005	
Ni	0.03	0.01	0.075		0.03		0.03	
Pb	<0.0001		<0.0001		0.008		0.001	
Ti	0.003		0.002		0.01		0.004	
V	0.002		0.004		0.003		0.006	
W	<0.0004		0.008		0.031		4.6	

*(a) reported from Anderson & Associates, Inc.
(b) reported from Chicago Spectro Service Laboratory, Inc.

treatment was intended to develop the same grain size for all the alloys. However, this could not be achieved due to the following reasons:

1. After grain size control treatment, the Fe-P and Fe-P-Mn alloys exhibit a phase transformation during cooling, while the Fe-P-Mo and Fe-P-W alloys remain in the same phase.
2. The conditions of the as-received alloys were too different. The Fe-P and Fe-P-Mn alloys had a very fine and equiaxed grain structure, while the Fe-P-Mo and Fe-P-W alloys had a very large and elongated grain structure.

Hence, the resulting grain size of the Fe-P-Mn alloy is significantly smaller when compared to those of the Fe-P, Fe-P-Mo, and Fe-P-W alloys. The problems arising from the grain size difference will be discussed later. The grain size control treatment was followed by tempering and aging treatments to vary the level of P, Mn, Mo, and W grain boundary segregation. The heat treatment conditions of the alloys are shown in Figure 3. In order to identify the type of alloy, aging temperature, and aging time, the specimens were designated with 5-digit numbers as:

X X X X X

type of alloy	aging temperature	aging time
0:Fe-P	40:400 °C	01:10 hrs
1:Fe-P-Mn	45:450	03:30
2:Fe-P-Mo	50:500	10:100
3:Fe-P-W	55:550	30:300
	60:600	

After each heat treatment a hardness measurement was made in HRB scale using a Wilson Rockwell hardness tester.

Recently, Kameda *et al.*[3,4] have developed a direct method to determine the critical local tensile stress necessary for the grain boundary brittle crack initiation (σ_c) using 4-point slow bend tests and tension tests, in conjunction with the Griffiths-Owen finite element elastic-plastic stress analysis.[33] In this study, the method developed by Kameda *et al.* will be adopted in order to determine the effect of P,

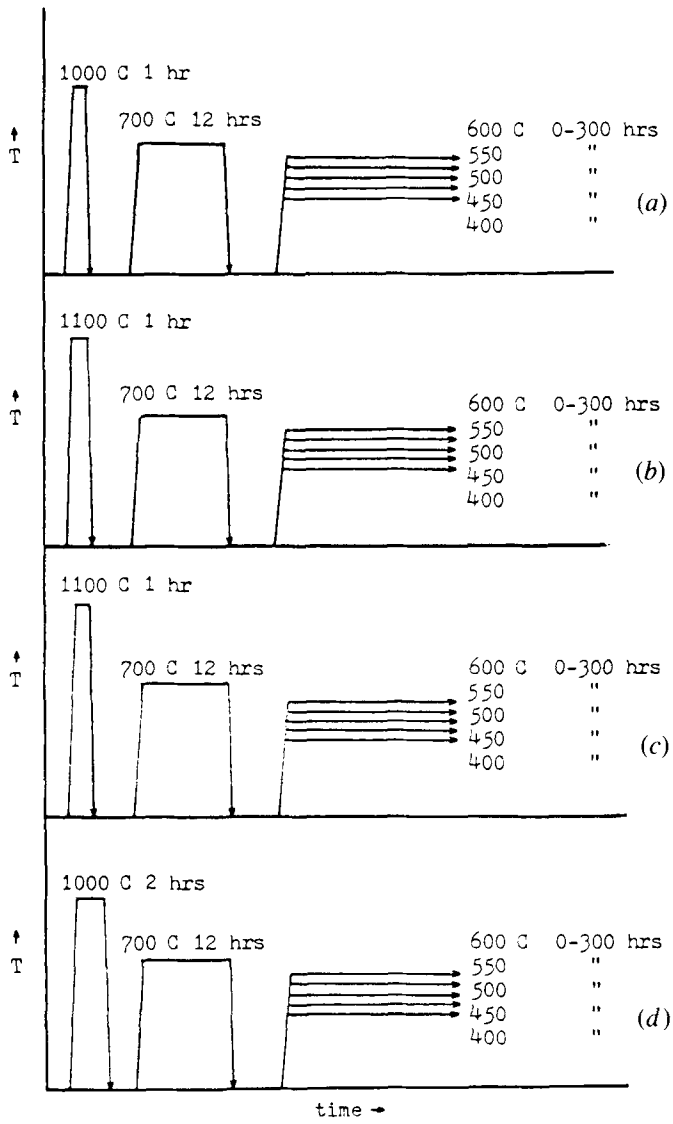

Fig. 3—Conditions of heat treatment for the (*a*) Fe-P, (*b*) Fe-P-Mn, (*c*) Fe-P-Mo, and (*d*) Fe-P-W alloys.

Mn, Mo, or W grain boundary segregation on the grain boundary strength. Hence, after heat treatments and hardness measurements, each rectangular block was cut into a notched bend test specimen and an unnotched tension test specimen. The geometry of the notched bend test specimen is the same as that used in the Griffiths-Owen analysis.

Both bend and tension tests were conducted using an Instron universal testing machine. The primary test temperatures were −140 °C for Fe-P and Fe-P-Mn alloys and −100 °C for Fe-P-Mo and Fe-P-W alloys. These test temperatures were chosen so the specimens fractured at initial yielding, but before general yielding in the bend test. In order to find the above test temperatures and the temperature dependence of yield stress (σ_y), some of the specimens of each alloy were tested over the temperature range of −196 °C to room temperature. All the test temperatures were obtained by controlling the amount of liquid nitrogen per unit time sprayed to the specimen and were monitored by a thermocouple embedded in the specimen. Cross-head speeds were 0.5 mm per minute for bend tests and 2 mm per minute for tension tests.

In order to determine the mode of fracture and the percentage of intergranular fracture (pct *IF*), the fractured bend test specimens were examined using scanning electron microscopy (SEM). For the estimation of pct *IF*, three SEM fractographs were taken for each specimen from the fracture surfaces located near the notch root in the center region of the specimen. Since the main interest is to find the fracture behavior in the area under σ_c, the distance from the notch root to the area where σ_c occurred (D_c) was determined for each specimen from the obtained nominal bending stress (σ_{nom}), σ_y, and the Griffiths-Owen analysis. Then, the line indicating the location of σ_c was drawn on the SEM fractograph. The pct *IF* was estimated by measuring the length of the line occupied by intergranular fracture surfaces. Figure 4 shows the examples of the fractographs used in the pct *IF* estimation.

For the determination of P, Mn, Mo, and W grain boundary concentration, Auger electron spectroscopy (AES) was employed. The Auger samples were prepared from the fractured bend test specimens. Auger samples were fractured *in situ* at the pressure of about 10^{-8} Pa and at the temperature of about −30 °C in the ultrahigh vacuum chamber of a scanning Auger spectrometer (Physical Electronics Industries model PHI 590). Auger spectra from the individual grain boundary facets were recorded as $dN(E)/dE$ *vs* E under the following conditions: 5 KeV, 300 to 500 nA, 2 μm primary beam; 3 V peak-to-peak modulation; 3 eV per second sweep rate; 0.3 second time constant. From the obtained Auger spectra quantitative estimates of grain boundary chemistry were made based on the method given in Reference 34. Auger sputtering depth profiles were also taken to examine whether P, Mn, Mo, and W are segregated locally at grain boundaries or tied up in a three dimensional (3D) second phase.

IV. RESULTS AND DISCUSSION

A. *The Effect of* Mn, Mo, *and* W *on* P *Grain Boundary Segregation*

As shown in Figure 5 the Auger sputtering depth profiles show that P, Mn, Mo, and W are concentrated locally at

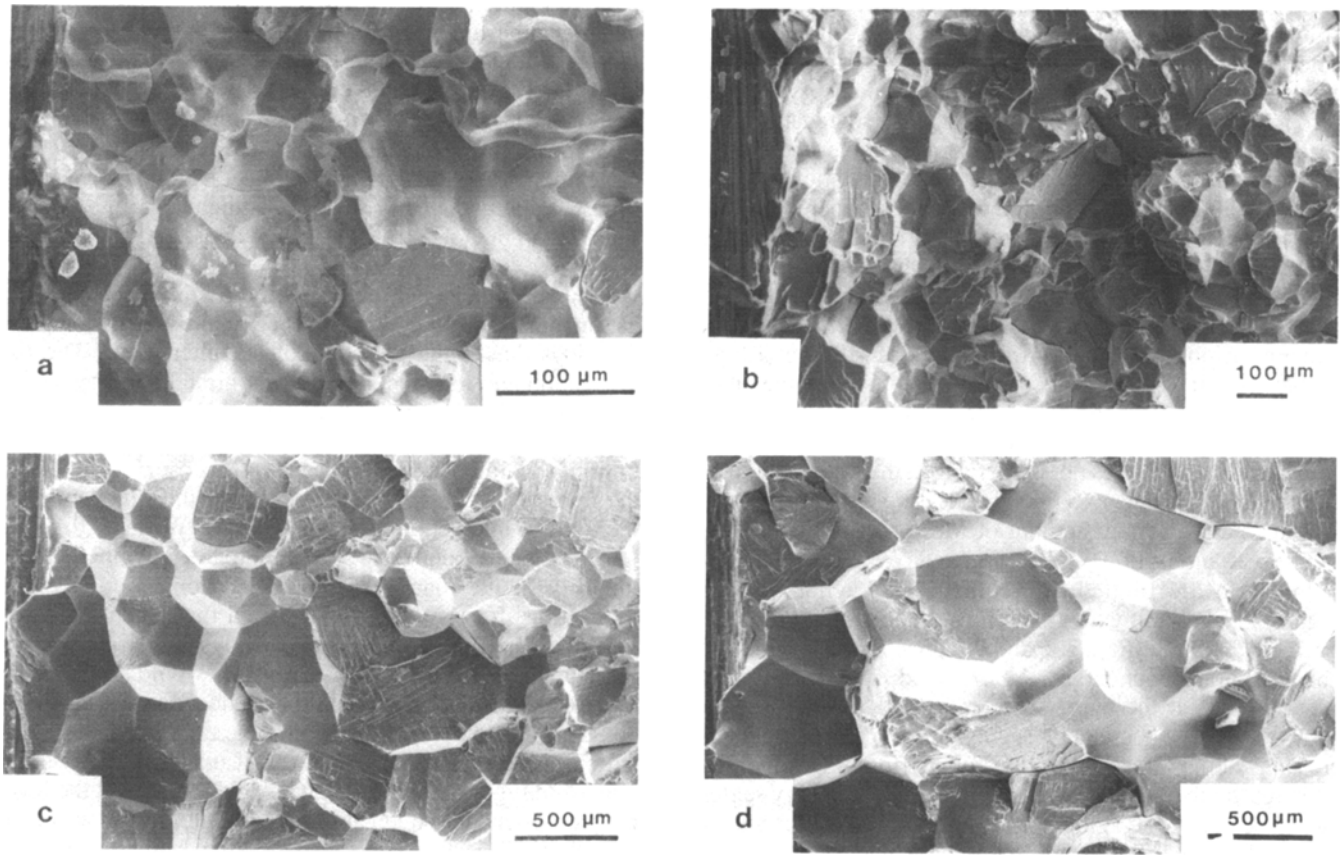

Fig. 4—Examples of the fractographs used in the estimation of the pct *IF*. (*a*) 05030, (*b*) 15530, (*c*) 25003, and (*d*) 35001 specimens.

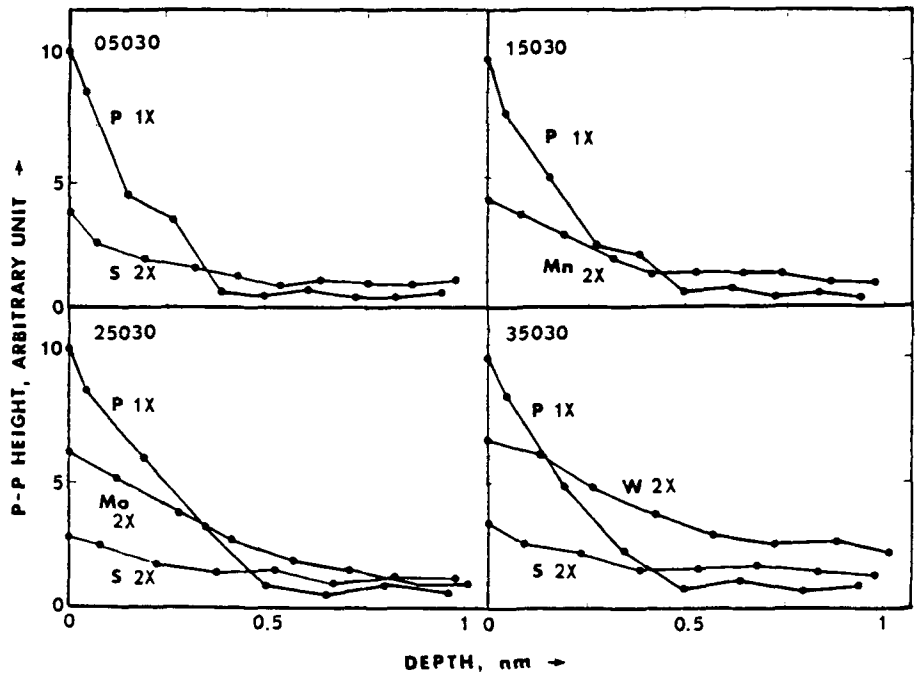

Fig. 5—Examples of the Auger sputtering depth profiles.

grain boundaries. This suggests that P, Mn, Mo, and W segregated at grain boundaries are not tied up in a 3D second phase. If they formed a 3D second phase at grain boundaries, their concentration profiles would extend over a much greater distance. The concentration profiles of Mo and W extend a little more than those of P and Mn. This is assumed to be because of the slower sputtering rate of Mo and W as pointed out previously by Schmerling *et al.*[35] It should be noted that this reduced sputtering rate of Mo or W would be expected from the grain boundary cohesive energy change associated with Mo and W grain boundary segregation. As described earlier, the grain boundary cohesive energy increases with Mo or W grain boundary segregation but decreases with P or Mn grain boundary segregation.

From Figure 5 it can be noted that a small amount of S grain boundary segregation occurs in the Fe-P, Fe-P-Mo, and Fe-P-W alloys, while S does not segregate to grain boundaries in the Fe-P-Mn alloy even though the S matrix concentration is virtually the same for all the alloys (Table III). It has been recognized that due to the very strong attractive S-Mn interaction, S is in general completely precipitated in the matrix of an Fe alloy containing Mn. This is why S does not participate in the grain boundary embrittlement problems of commercial Fe alloys which always contain a certain amount of Mn for that purpose.

The variations of P, Mn, Mo, and W grain boundary segregation are plotted as a function of aging time in Figure 6 and as a function of aging temperature in Figure 7. Each data point in Figures 6 and 7 represents the average of about 10 grain boundaries. As expected, it is found from Figure 6 that at the aging temperature of 500 °C, P, Mn, Mo, or W grain boundary segregation increases with increasing aging time. It is also found from Figure 7 that with 300 hours aging the maximum P grain boundary segregation occurs at the aging temperature of 500 °C for all the alloys. Seah's recent study[36] on the kinetics of P grain boundary segregation in an Fe-Cr-Ni-C alloy has also shown that with 300 hours aging the maximum P grain boundary segregation can be obtained at the aging temperature of about 500 °C. In the case of alloying elements it can be seen from Figure 7 that the aging temperature for the maximum grain boundary segregation after 300 hours aging is also 500 °C for Mo and W, but is 550 °C for Mn.

From Figures 6 and 7 it can be seen that for a given aging treatment the amount of Mn, Mo, or W grain boundary segregation is somewhat less than that of P grain boundary segregation even though the Mn, Mo, or W matrix concentration is much higher than P. This suggests that Mn, Mo, or W possesses a much lower grain boundary segregation enrichment ratio than P. Here, it should be noted from Figure 6 that in the early stages of aging the grain boundary segregation rate of Mn, Mo, or W is apparently slower than that of P.

It has been believed that impurity grain boundary segregation is influenced by the presence of alloying elements in Fe alloys due to the existence of *I-A* interaction. The *I-A* interaction and its effect on impurity grain boundary segregation have been explained by the Guttmann model.[2] According to the Guttmann model, Cr, Mn, and Ni enhance impurity grain boundary segregation by cosegregating with the impurity to grain boundaries due to their moderate attractive *I-A* interaction, while Mo, Ti, V, W, and Zr reduce impurity grain boundary segregation by precipitating the impurity in the matrix due to their strong attractive *I-A* interaction. It was therefore expected that when the Fe-P, Fe-P-Mn, Fe-P-Mo, and Fe-P-W alloys were selected for this study, P grain boundary segregation would be enhanced in the Fe-P-Mn alloy and would be reduced in the Fe-P-Mo and Fe-P-W alloys compared to P grain boundary segregation in the Fe-P alloy. However, it is of great interest to note from Figure 8 that for a given aging treatment the level of grain boundary segregation is basically the same for all the alloys. This fact could suggest that P grain boundary segregation is not affected by the presence of Mn, Mo, or W,

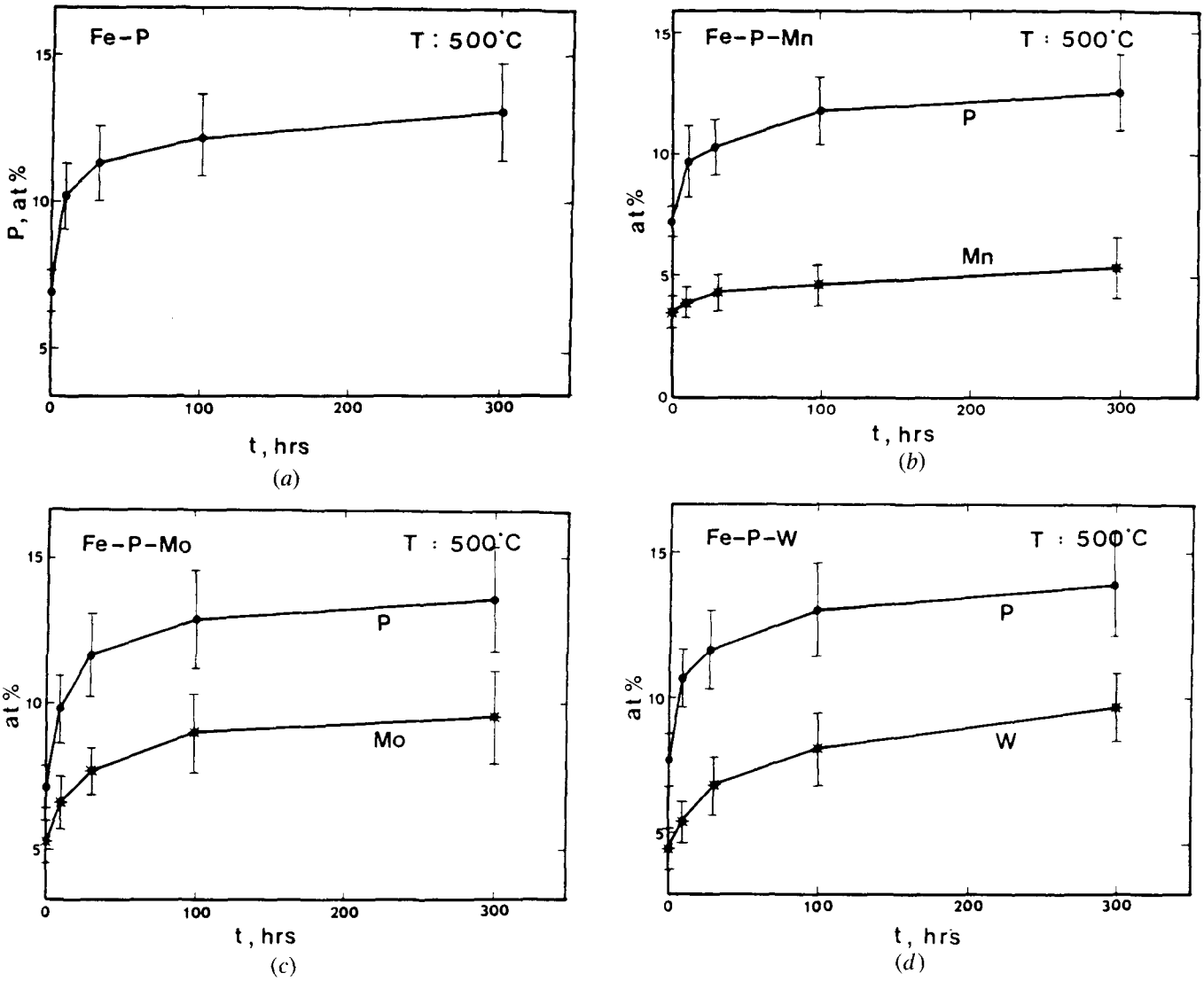

Fig. 6—The variation of P, Mn, Mo, or W grain boundary segregation with aging time in the (*a*) Fe-P, (*b*) Fe-P-Mn, (*c*) Fe-P-Mo, and (*d*) Fe-P-W alloys.

and that Mn, Mo, or W does segregate to grain boundaries simultaneously with P but independently of P. Since the alloys have different grain size, the P diffusion distances must be considered in order to examine if P grain boundary segregation may be affected by the difference in grain size. Gruzin and Minal[37] have obtained the diffusivity of P in Fe as:

$$D_P^{Fe} = 7 \times 10^{-7} \exp(-20{,}130/T) \text{ m}^2/\text{sec} \quad [3]$$

With 300 hours aging treatment the calculated P diffusion distances are 0.28 μm and 8.55 μm for the aging temperatures of 400 and 600 °C, respectively. These values are much less than the grain diameters of the alloys used in this study. The grain diameters of the alloys are 50 to 700 μm as shown in Figure 4. Therefore, the grain size effect on P grain boundary segregation would be negligible even though the grain boundary area/volume ratio varies with grain size. Based upon his experimental study on the grain size effect, Guttmann[31] has also claimed that grain boundary segregation itself does not vary with grain size.

Recently, Briant[38] has conducted a grain boundary segregation study by systematically varying the matrix concentrations of Cr, Mn, and Ni in P-doped Fe alloys. His results have also shown that the changes in the matrix concentrations of Cr, Mn, and Ni do not influence P grain boundary segregation. Based upon his experimental results, he has claimed that P grain boundary segregation is independent of Cr, Mn, and Ni grain boundary segregation. Hence, it can be concluded from the results of this study and of Briant's that P and alloying elements segregate to grain boundaries independently and that P grain boundary segregation is thereby not influenced by the presence of alloying elements.

B. *The Effect of* Mn, Mo, *and* W *on Grain Boundary Embrittlement*

As mentioned earlier, the mechanical-structural factors which are also very important variables controlling grain boundary embrittlement could not be effectively controlled in this study; the Fe-P, Fe-P-Mn, Fe-P-Mo, and Fe-P-W alloys have different grain size and hardness. However, the values of grain size and hardness are virtually identical for all the specimens of each alloy after the different aging treatments. Therefore, it is intended that in the following

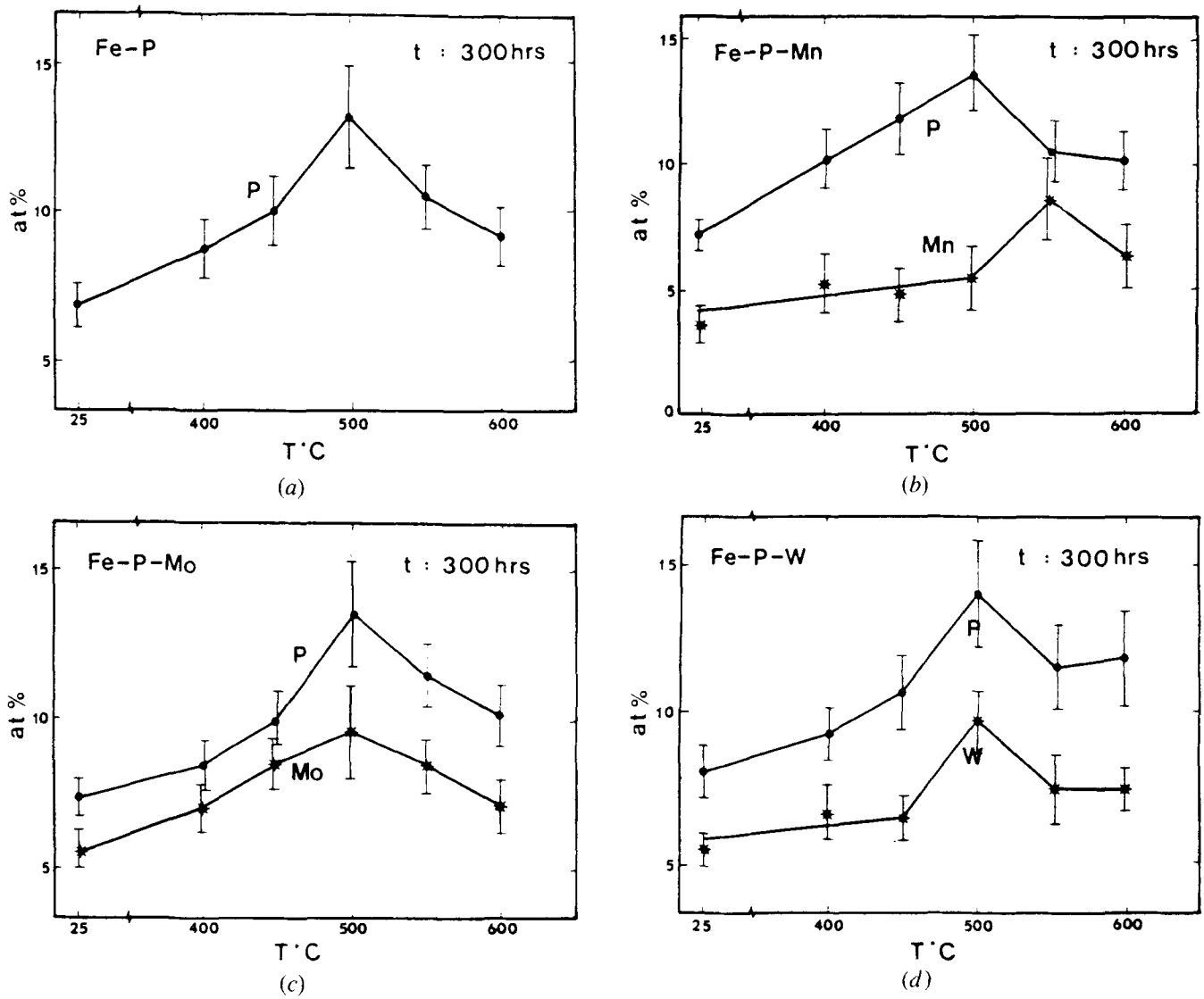

Fig. 7—The variation of P, Mn, Mo, or W grain boundary segregation with aging temperature in the (*a*) Fe-P, (*b*) Fe-P-Mn, (*c*) Fe-P-Mo, and (*d*) Fe-P-W alloys.

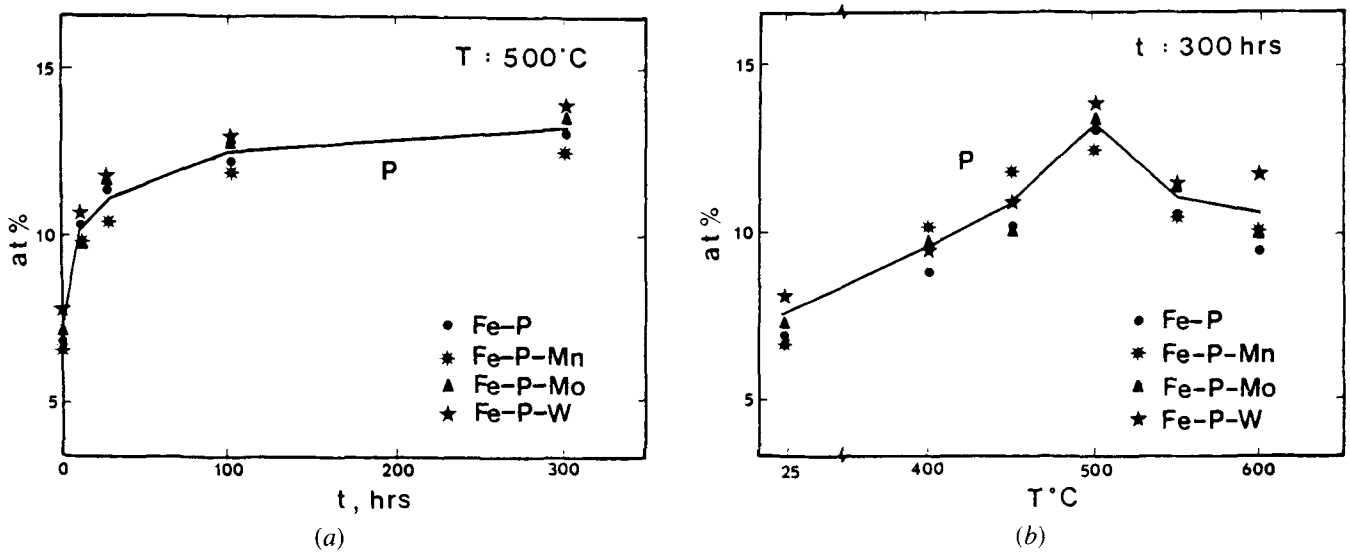

Fig. 8—The variation of P grain boundary segregation (*a*) with aging time and (*b*) with aging temperature in the Fe-P, Fe-P-Mn, Fe-P-Mo, and Fe-P-W alloys.

discussion the comparison of the experimental results will focus on the individual alloys.

The results of hardness, bend, and tension tests are summarized in Table IV. It can be seen that for a given test temperature σ_y is virtually identical for all the specimens of each alloy, but varies with the test temperature. Figure 9 shows that the temperature dependence of σ_y becomes large at the test temperature below about −100 °C and that the large temperature dependence for the Fe-P-Mo and Fe-P-W alloys occurs at higher test temperatures than those for the Fe-P and Fe-P-Mn alloys.

From the values of σ_{nom} and σ_y in Table IV, the critical local tensile stress necessary for the grain boundary brittle crack initiation (σ_c) and the distance from the notch root to the region of $\sigma_c(D_c)$ were calculated using the Griffiths-Owen analysis.[33] Figure 10 shows the variations of σ_c and

Table IV. Hardness, Bend, and Tension Test Results of the Fe-P, Fe-P-Mn, Fe-P-Mo, and Fe-P-W Alloys

Specimen	HRB	T(°C)	σ_{nom} (MPa)	Pct *IF*	T(°C)	σ_y (MPa)	σ_{fr} (MPa)	Pct e
00000	38	−140	527	53	−140	305	409	1.9
04001	38	−196	623	*	−160	419	446	1.1
04003	36	−140	511	61	25	119	131	59.2
04010	40	−100	*	*	− 80	161	*	*
04030	36	−140	494	58	−140	305	397	2.9
04503	37	−140	460	57	−140	293	335	1.1
04510	39	−140	482	67	−140	300	310	0.9
04530	34	−140	490	57	−140	300	305	0.9
05001	38	−196	603	*	−140	300	325	1.0
05003	38	−140	482	70	−140	300	312	0.9
05010	38	−140	423	85	−140	*	268	0.7
05030	35	−140	393	98	−140	*	260	0.6
05501	39	−140	494	68	−160	*	365	0.8
05503	38	−140	473	75	*	*	*	*
05510	37	−140	489	74	− 80	149	*	*
05530	37	−140	460	75	−140	303	315	0.9
06001	38	−140	519	50	−160	*	355	0.8
06003	37	−140	519	82	− 80	156	*	*
06010	36	−140	519	61	*	*	*	*
06030	36	−140	511	95	−140	298	360	1.2
10000	68	−140	887	32	−140	379	689	4.4
14001	64	−120	*	*	−160	476	707	2.3
14003	65	−196	536	*	−100	273	*	*
14010	65	−196	493	*	*	*	*	*
14030	65	−140	783	45	−140	367	675	4.2
14503	64	−140	858	48	*	*	*	*
14510	65	−140	741	49	−160	471	471	1.0
14530	65	−140	720	46	−140	379	694	4.0
15001	66	−140	728	42	−140	419	699	3.5
15003	66	−140	657	48	−140	434	665	3.4
15010	65	−140	603	60	−140	432	594	2.5
15030	66	−140	544	79	−140	429	558	1.6
15503	66	−140	720	38	*	*	*	*
15510	66	−140	552	58	*	*	*	*
15530	66	−140	502	81	−140	402	511	1.5
16003	66	−196	552	*	*	*	*	*
16010	65	−196	460	*	25	181	179	49.9
16030	59	−140	695	53	−140	362	684	3.1
20000	68	−100	561	38	−100	315	454	2.2
24010	67	−100	490	39	−120	377	389	0.9
24030	68	−100	531	34	−100	315	422	1.8
24501	67	− 80	*	*	−140	*	377	0.7
24503	68	−100	494	41	− 80	265	434	3.1
24510	67	−100	536	45	− 80	263	417	2.2
24530	68	−100	557	36	−100	327	434	1.8
25001	68	−100	473	47	−100	310	360	1.2
25003	67	−100	419	55	−100	*	285	0.6
25010	68	−100	485	48	−100	308	315	0.9
25030	67	−100	502	40	−100	310	402	1.5
25501	69	−100	515	33	−100	*	407	0.8
25503	65	−100	427	26	−100	*	288	0.7
25510	69	−100	494	45	−100	325	404	1.3
25530	67	−100	523	41	−100	320	417	1.7
26001	68	−120	737	*	25	146	298	43.5
26003	67	− 80	*	*	− 50	206	*	*
26010	70	−100	490	35	*	*	*	*

Table IV. Cont. Hardness, Bend, and Tension Test Results of the Fe-P, Fe-P-Mn, Fe-P-Mo, and Fe-P-W Alloys

Specimen	HRB	T(°C)	σ_{nom} (MPa)	Pct *IF*	T(°C)	σ_y (MPa)	σ_{fr} (MPa)	Pct e
26030	70	−100	494	28	−100	310	417	1.5
30000	71	−100	674	41	−100	342	449	1.8
34001	70	−100	728	31	−160	*	429	0.9
34003	71	−100	661	38	− 80	270	441	3.8
34010	71	−100	670	44	*	*	*	*
34030	67	−100	720	44	−100	340	417	1.2
34501	70	−100	707	46	−120	397	414	1.0
34503	69	−100	665	36	− 80	253	*	*
34510	72	−100	665	43	*	*	*	*
34530	67	−100	661	60	−100	332	379	1.2
35001	68	−100	557	66	−100	*	332	0.7
35003	69	−100	636	50	−100	337	337	0.8
35010	70	−100	661	48	−100	337	402	1.1
35030	67	−100	674	46	−100	355	417	1.3
35503	71	−100	624	67	−100	*	310	0.7
35510	71	−100	653	55	−100	352	372	0.9
35530	70	−100	657	44	−100	340	389	1.0
36001	71	−100	619	28	25	154	347	39.9
36003	70	−100	628	53	−100	397	422	1.1
36010	71	−100	653	60	*	*	*	*
36030	71	−100	657	47	−100	337	409	1.2

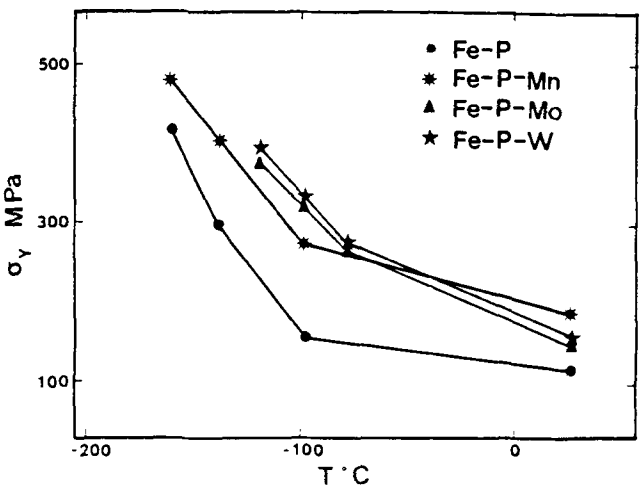

Fig. 9 — The temperature dependence of yield stress in the Fe-P, Fe-P-Mn, Fe-P-Mo, and Fe-P-W alloys.

D_c with aging time at the aging temperature of 500 °C. With increasing aging time, for the Fe-P and Fe-P-Mn alloys σ_c and D_c decrease in the whole range of aging time, but for the Fe-P-Mo and Fe-P-W alloys they decrease in the early stages of aging and then increase in the later stages of aging. The variations of σ_c and D_c with aging time in the Fe-P-Mo and Fe-P-W alloys look anomalous, but these could have arisen from the remedial effect of Mo or W on P-induced grain boundary embrittlement which can be predicted from the extended model; the earlier P grain boundary segregation weakens grain boundaries and the subsequent Mo or W grain boundary segregation strengthens the weakened grain boundaries. It was already noted from Figure 6 that in the early stages of aging the grain boundary segregation rate of P is apparently faster than that of Mo or W. The remedial effect of Mo and W will be further considered later.

It can be noted from Table IV that for each alloy the values of σ_{nom}, tensile fracture stress (σ_{fr}), and pct elongation (pct e) show the similar variations with aging time to those of σ_c and D_c, while the variation of pct *IF* with aging time shows the very opposite of those of σ_c, D_c, σ_{nom}, σ_{fr}, and pct e.

Before σ_c is correlated to the P, Mn, Mo, and W grain boundary segregation to observe the effect of P, Mn, Mo, and W grain boundary segregation on the change in σ_c, it needs to be briefly considered how σ_c can be regarded as the grain boundary strength. It has been suggested that brittle fracture in a deformable solid may be thought of as a three-stage process which can lead to a three-fold fracture criterion.[3] The three stages are the following:

1. A microcrack nucleates at an obstacle (*i.e.*, a second phase precipitate, inclusion, grain boundary, *etc.*) due to the blockage of a slip band or twin. For this first stage, at least local yielding is required.
2. The microcrack initiates its propagation beyond the obstacle. Hence, a certain value of $\sigma_{22}^{max} \simeq \sigma_c$ is required depending on the plastic work of fracture (γ_p).
3. The propagating microcrack leads to the long range propagation. This depends on the gradient in the maximum principal stress.

Now, the above three-fold fracture criterion will be combined with the following assumptions:[4]

1. There is one grain boundary facet per grain which is oriented essentially normal to σ_{22}.
2. The nucleated microcrack initiates its propagation along the embrittled grain boundary in the region of σ_{22}^{max}.
3. The first grain boundary along which the microcrack propagates triggers unstable fracture of the specimen.

Then, σ_c can be considered as the critical local tensile stress necessary for the initiation of the grain boundary brittle fracture which is equivalent to the grain boundary strength.

Recently, Jokl *et al.*[39,40] have developed a Griffith-type fracture criterion assuming that the two processes of bond

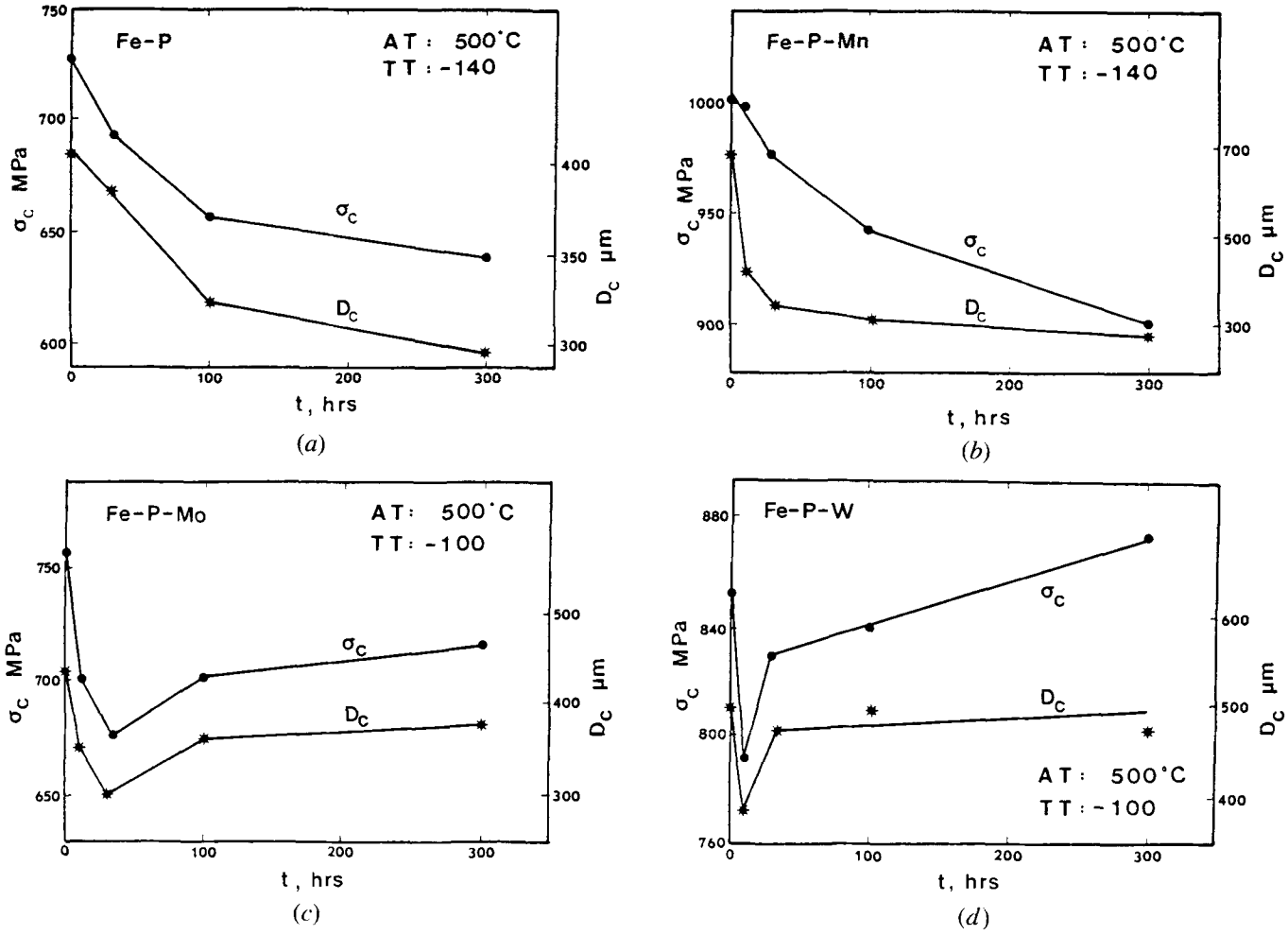

Fig. 10—The variations of the critical local tensile stress for grain boundary brittle crack initiation (σ_c) and the distance from the notch root to the region of σ_c with aging time in the (*a*) Fe-P, (*b*) Fe-P-Mn, (*c*) Fe-P-Mo, and (*d*) Fe-P-W alloys.

breaking and dislocation emission occur concomitantly at the tip of a microcrack during brittle fracture of a deformable solid. This criterion suggests that the plastic work of fracture and the microcrack stress intensity are directly related to the ideal work of fracture. They have also proposed that the microcrack stress intensity at fracture would be related to σ_c in the form:

$$k_{FR}^2 = (\sigma_c\sqrt{\pi c})^2 + [f(\sigma_c, c, l, \tau)]^2 \qquad [4]$$

where c is the length of the microcrack, l is the length of the initial dislocation pile-up that nucleates the microcrack, and τ is the lattice friction stress for dislocation motion. Therefore, it would be expected that the grain boundary strength is directly related to the ideal work of fracture which is equivalent to the grain boundary cohesive energy.

Combining the information of the grain boundary strength with the grain boundary chemistry, the variation of the grain boundary strength may be considered for each alloy as a function of the amount of P, Mn, Mo, or W grain boundary segregation. As mentioned earlier, a very small amount of S grain boundary segregation occurs in Fe-P, Fe-P-Mo, and Fe-P-W alloys. However, the amount of S grain boundary segregation does not much vary with different aging treatments for each alloy. Therefore, the effect of S on the grain boundary strength would be about the same for all the specimens of each alloy, and the grain boundary strength change would mainly be attributed to the change in P, Mn, Mo, or W grain boundary segregation for the specimens of each alloy.

Figure 11 shows the variation of grain boundary strength with the amount of P grain boundary segregation. It can be seen that the grain boundary strength decreases with increasing P grain boundary segregation in the Fe-P alloy and in the Fe-P-Mn, Fe-P-Mo, or Fe-P-W alloy for a given Mn, Mo, or W grain boundary segregation. The variation of the grain boundary strength is plotted for the Fe-P-Mn, Fe-P-Mo, or Fe-P-W alloy as a function of Mn, Mo, or W grain boundary segregation in Figure 12. It can be noted from Figure 12 that for a given P grain boundary segregation the grain boundary strength decreases with increasing Mn grain boundary segregation and increases with increasing Mo or W grain boundary segregation. Since, as discussed earlier, the grain boundary cohesive energy would be directly related to the grain boundary strength, the grain boundary cohesive energy would show the similar variation with P, Mn, or W grain boundary segregation to that of the grain boundary strength; the grain boundary cohesive energy would decrease with increasing P or Mn grain boundary segregation and would increase with increasing Mo or W grain boundary segregation. These experimental

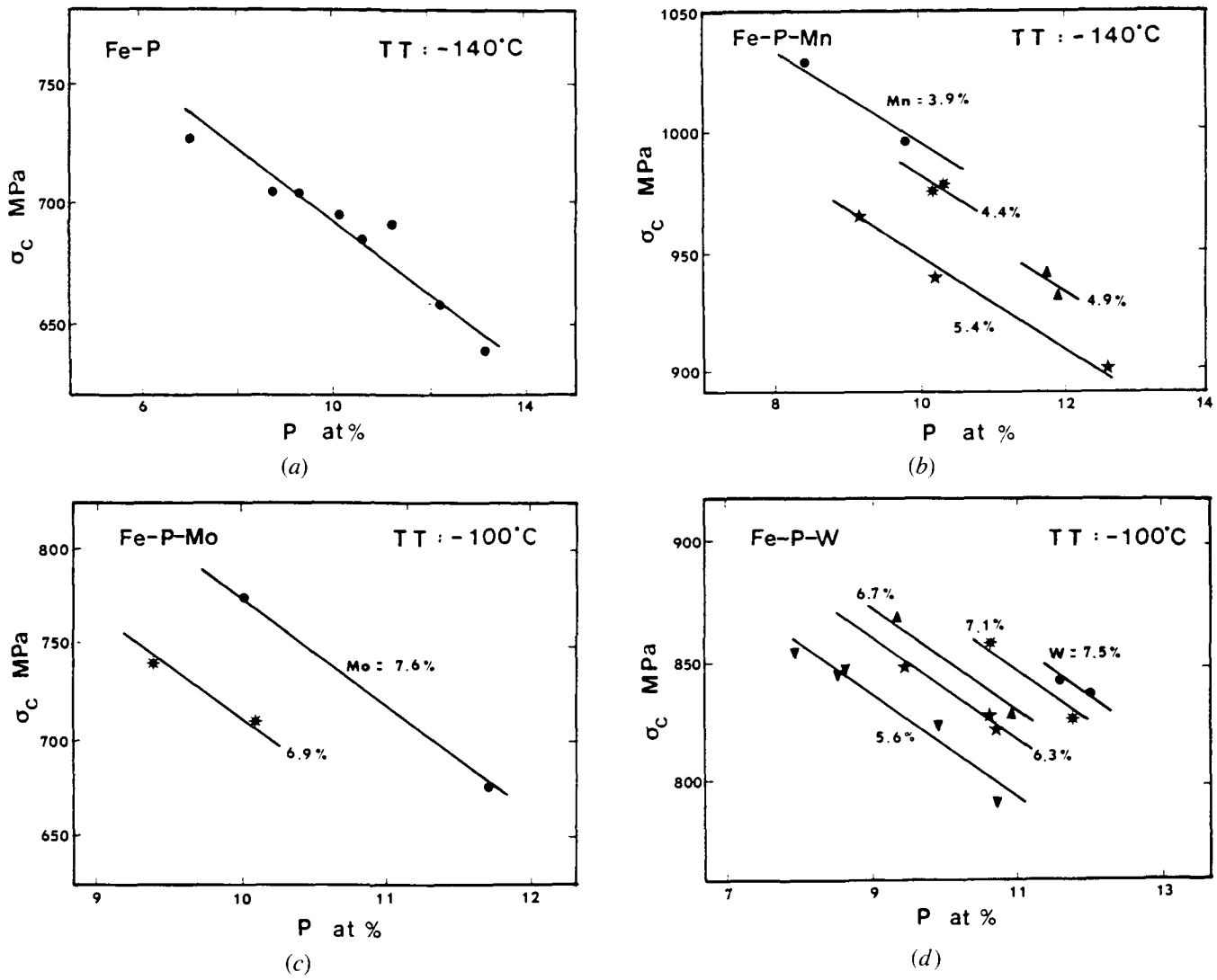

Fig. 11 — The variation of the grain boundary strength with P grain boundary segregation in the (*a*) Fe-P, (*b*) Fe-P-Mn, (*c*) Fe-P-Mo, and (*d*) Fe-P-W alloys.

results are consistent with the original and extended nonequilibrium models. The reduced grain boundary cohesive energy due to P grain boundary segregation was predicted from the original model, and the embrittling effect of Mn and the remedial effect of Mo and W on P-induced grain boundary embrittlement in the Fe-P-Mn, Fe-P-Mo, and Fe-P-W alloys were predicted from the extended model.

As discussed previously, the effect of alloying elements on P-induced grain boundary embrittlement could also be explained by the effect of alloying elements on the P embrittling potency determined by their relative electronegativities to P and Fe.[30] This idea could be promising to reveal the interaction between impurities and alloying elements at the grain boundary and its effect on grain boundary embrittlement. This study did not intend to confirm experimentally this idea. The results from an AES and ionization loss spectroscopy study have suggested some evidences of the above effect, but still are not quite satisfactory.[26] More research efforts are necessary to establish fully the *I-A* cross-effect on the embrittling and remedial effects of impurities and alloying elements.

V. CONCLUSIONS

1. The extended nonequilibrium model can directly and simply predict the effect of alloying elements on the impurity-induced grain boundary embrittlement in terms of the grain boundary cohesive energy. The extended model suggests that Mo, W, and Zr strongly reduce, Ni, Ti, and V slightly reduce, and Cr and Mn enhance impurity-induced grain boundary embrittlement in an Fe-*I*-*A* system. In this study the predictions were made only for an Fe-*I*-*A* system, but the extended model can be applied to all the materials which encounter a grain boundary embrittlement problem associated with grain boundary segregation of the substitutional solutes. This model is also applied to the impurity-induced interfacial embrittlement in a metal matrix composite containing low impurity solubility fibers.
2. The experimental results on the Fe-P, Fe-P-Mn, Fe-P-Mo, and Fe-P-W alloys show that for a given P grain boundary segregation the grain boundary strength decreases with the Mn grain boundary segregation and

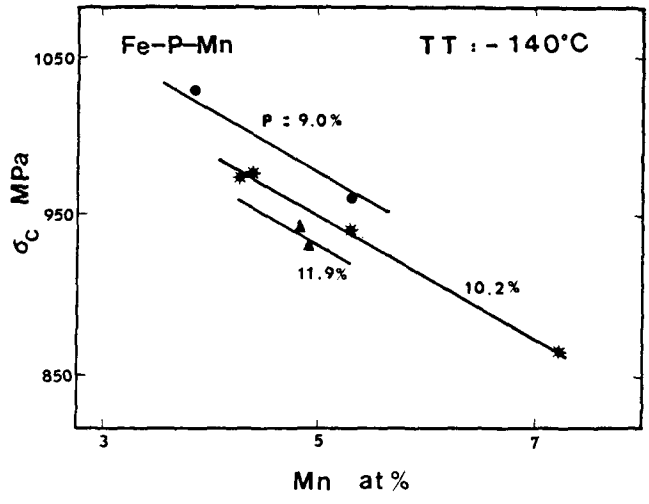

(*a*)

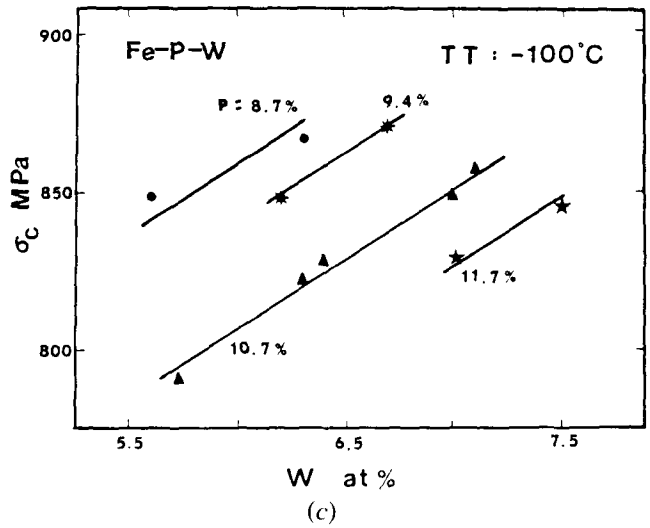

(*c*)

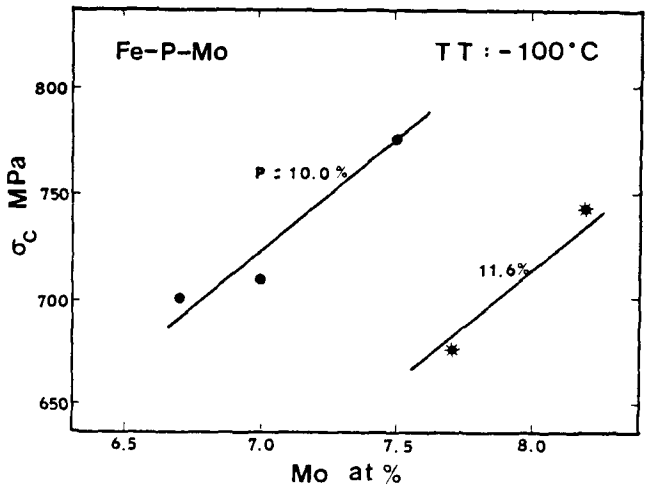

(*b*)

Fig. 12—The variation of the grain boundary strength with Mn, Mo, or W grain boundary segregation in the (*a*) Fe-P-Mn, (*b*) Fe-P-Mo, and (*c*) Fe-P-W alloys.

increases with Mo or W grain boundary segregation, which is consistent with the predictions from the extended model.

3. The grain boundary strength decreases with P grain boundary segregation in the binary Fe-P alloy. Also, for a given Mn, Mo, or W grain boundary segregation the grain boundary strength decreases with P grain segregation in the Fe-P-Mn, Fe-P-Mo, or Fe-P-W alloy.
4. P grain boundary segregation is not influenced by the presence of Mn, Mo, or W in the Fe alloy. Mn, Mo, or W grain boundary segregation occurs simultaneously with P grain boundary segregation; but Mn, Mo, or W grain boundary segregation is independent of P grain boundary segregation.
5. In the Fe-P, Fe-P-Mn, Fe-P-Mo, or Fe-P-W alloy, with 300 hours aging treatment, the maximum P, Mo, or W grain boundary segregation occurs at 500 °C, while the maximum Mn grain boundary segregation occurs at 550 °C.
6. In the early stages of aging treatment, the grain boundary segregation rate of Mn, Mo, or W is apparently slower than that of P in the Fe-P-Mn, Fe-P-Mo, or Fe-P-W alloy.
7. With increasing aging time at 500 °C, the grain boundary strength decreases for the Fe-P and Fe-P-Mn alloys; but for the Fe-P-Mo and Fe-P-W alloys the grain boundary strength decreases in the early stages of aging and then increases in the later stages of aging. This anomalous variation in the Fe-P-Mo and Fe-P-W alloys is caused by the remedial effect of Mo and W on P-induced grain boundary embrittlement (*i.e.*, the earlier P grain boundary segregation weakens grain boundaries and then the subsequent Mo or W grain boundary segregation strengthens the weakened grain boundaries).

APPENDIX A

List of symbols

Superscript

B	boundary region in a grain boundary (see Figure 1)
BM	boundary matrix interface region in a grain boundary (see Figure 1)
f	final state
F	fiber in a composite material
GB	grain boundary which consists of *B* and *BM*
i	initial state
I	interface region in a composite material (see Figure A1)
M	matrix (see Figures 1 and A1)
T	total system

Nomenclature

A	interfacial area
c	microcrack length
D_c	distance from the notch root to the region σ_c

D_P diffusion coefficient of P
G Gibb's free energy
H enthalpy
$\underline{H}_j$ molar enthalpy of pure element j
$\overline{H}_j$ partial molar enthalpy of component j ($\overline{H}_j = \delta H/\delta N$)
${}^m\overline{H}_j$ partial molar mixing enthalpy of component j (${}^m\overline{H}_j = \overline{H}_j - \underline{H}_j$)
H_j^* sublimation enthalpy of pure element j per unit area
k_{FR} microcrack stress intensity at fracture
l length of the initial dislocation pile-up
N_j number of moles of component j
s interfacial tension
S entropy
X_j molar fractional monolayer of component j
Z coordination number
γ ideal work of fracture
μ_j chemical potential of component j
σ_c critical local tensile stress
σ_{fr} tensile fracture stress
σ_{nom} nominal bending stress
σ_y tensile yield stress
σ_{22}^{max} maximum principal stress

APPENDIX B

The extension of the nonequilibrium model to Fe-*I*-*A* ternary systems

By the definition of the Gibb's free energy (*i.e.*, $G = H - TS$), the total Gibb's free energy change during the grain boundary segregation process can be expressed as:

$$\delta G^T = \delta H^T - T\,\delta S^T \qquad [B1]$$

where H^T and S^T are total enthalpy and entropy of the system, respectively. Since the configuration entropy does not contribute to the grain boundary cohesive energy[1] and the contribution of the vibrational entropy to the grain boundary cohesive energy is negligible,[7] the enthalpy change in the grain boundary region during the grain boundary segregation process is equivalent to the grain boundary cohesive energy change associated with grain boundary segregation.

The total enthalpy of the system consisting of the boundary (B), boundary matrix interface (BM), and matrix (M) regions as shown in Figure 1 can be described as the sum of the enthalpy of each region since enthalpy is an extensive thermodynamic variable:

$$H^T = H^B + H^{BM} + H^M \qquad [B2]$$

From Eq. [B2] the total enthalpy change of the system during grain boundary segregation can be expressed as the sum of the enthalpy change of each region:

$$\delta H^T = \delta H^B + \delta H^{BM} + \delta H^M \qquad [B3]$$

Here, we are mainly interested in the enthalpy change in the grain boundary region since this is directly equivalent to the grain boundary cohesive energy change associated with grain boundary segregation. Hence, by rearranging Eq. [B3], we obtain the grain boundary cohesive energy change associated with grain boundary segregation as:

$$\delta H^{GB} = \delta H^B + \delta H^{BM} = \delta H^T - \delta H^M \qquad [B4]$$

The terms δH^T and δH^M in Eq. [B4] have been calculated by Stark and Marcus.[1] For a multi-component system the terms δH^T and δH^M can be expressed as:

$$\delta H^T = \delta H_*^B + \delta H_*^{BM} \qquad [B5]$$

$$\delta H^M = \underline{H}_1^M\,\delta N_1^M + \sum_{j=2}^{n} \overline{H}_j^M\,\delta N_j^M \qquad [B6]$$

where $\underline{H}_1^M$ is the molar enthalpy of the pure solvent 1 in M, $\overline{H}_j^M$ is the partial molar enthalpy of the solute j in M, δN_1^M is the change in the number of moles of 1 in M, and δN_j^M is that of j in M. The terms δH_*^B and δH_*^{BM} in Eq. [B5] are the enthalpy changes in B and BM, respectively, when B and BM are transformed from their initial high energy state to their final low energy state. This transformation is equivalent to the system undergoing grain boundary segregation as an attempt to obliterate the high grain boundary energy. A better understanding of these terms may be obtained from the details of the development of Eqs. [B5] and [B6] presented in Reference 1.

Assuming that each solute atom displaces one solvent atom from B or BM to M when solute atoms segregate from M to B or BM, we may find that the sum of the changes in the number of moles of solvent and solutes in M is zero:

$$\delta N_1^M + \sum_{j=2}^{n} \delta N_j^M = 0 \qquad [B7]$$

The above assumption is at least approximately true for a grain boundary segregation process of the substitutional solutes. Therefore, the following analysis can be applied only to the substitutional solutes segregating to grain boundaries.

Substituting Eq. [B7] to Eq. [B6], we obtain:

$$\delta H^M = \sum_{j=2}^{n} (\overline{H}_j^M - \underline{H}_1^M)\,\delta N_j^M \qquad [B8]$$

By using the partial molar mixing enthalpy term which is defined as ${}^m\overline{H}_j^M = \overline{H}_j^M - \underline{H}_j^M$, Eq. [B8] can be rewritten as:

$$\delta H^M = \sum_{j=2}^{n} ({}^m\overline{H}_j^M + \underline{H}_j^M - \underline{H}_1^M)\,\delta N_j^M \qquad [B9]$$

Now, combining Eqs. [B4], [B5], and [B9], we may obtain the grain boundary cohesive energy change during grain boundary segregation for a multicomponent system as:

$$\begin{aligned}\delta H^{GB} &= \delta H^B + \delta H^{BM} \\ &= \delta H_*^B + \delta H_*^{BM} - \sum_{j=2}^{n} ({}^m\overline{H}_j^M + \underline{H}_j^M - \underline{H}_1^M)\,\delta N_j^M\end{aligned} \qquad [B10]$$

The main purpose of this analysis is to study the effect of alloying elements on impurity-induced grain boundary embrittlement in Fe alloys. Hence, Eq. [B10] will be applied to an Fe-*I*-*A* ternary system. For an Fe-*I*-*A* ternary system, Eq. [B10] can be rewritten as:

$$\begin{aligned}\delta H^{GB} &= \delta H^B + \delta H^{BM} \\ &= \delta H_*^B + \delta H_*^{BM} - ({}^m\overline{H}_I^M + \underline{H}_I^M - \underline{H}_{Fe}^M)\,\delta N_I^M \\ &\quad - ({}^m\overline{H}_A^M + \underline{H}_A^M - \underline{H}_{Fe}^M)\,\delta N_A^M\end{aligned} \qquad [B11]$$

By using Eq. [B11], it is now possible to estimate numerically the effect of alloying elements on impurity-induced grain boundary embrittlement using the published thermodynamical data on the molar enthalpies, the partial molar mixing enthalpies, and the measured grain boundary chemistry with the proper assumption on the terms δH_*^B and δH_*^{BM}.

APPENDIX C

The segregation effect on interfacial cohesion in composite materials

The nonequilibrium model which describes the influence of grain boundary segregation on the grain boundary cohesive energy can be applied to the interfacial embrittlement problems associated with impurity interfacial segregation in continuous fiber metal matrix composite materials. The nonequilibrium model has been modified for the application to composite materials[41] by adopting most of the basic assumptions used for the development of the nonequilibrium model with some other assumptions which are suitable for the nature of composite materials.

The total Gibb's free energy of a multicomponent system which consists of the matrix (M), interface (I), and fiber (F) as shown in Figure A1 can be given as:

$$G^T = \sum_{j=1}^{n} \sum_{k} \mu_j^k N_j^k + s^I A^I \qquad [C1]$$

where μ_j^k is the chemical potential of component j in k ($k = M$, I, or F), N_j^k is the number of moles of j in k, s^I is the interfacial tension, and A^I is the interfacial area. Assuming that F is made of pure element and defining that the component 1 is the solvent in M, the components 2 to $n-1$ are the solutes in M and the component n is the element of pure solid F, we may rewrite Eq. [C1] as:

$$G^T = \sum_{j=1}^{n-1} \sum_{q} \mu_j^q N_j^q + \mu_n^F N_n^F + s^I A^I \qquad [C2]$$

where q is M or I.

With the following three assumptions: (1) interfacial segregation takes place at the constant interfacial area, temperature, and pressure, (2) entropy production during the interfacial segregation process is negligible, and (3) no flux occurs between F and M or I during the interfacial segregation (*i.e.*, $\mu_n^{fF} = \mu_n^{iF}$ and $N_n^{fF} = N_n^{iF}$), we may describe the total Gibb's free energy change associated with interfacial segregation as:

$$\delta G^T = \sum_{j=1}^{n-1} \sum_{q} (\mu_j^{fq} N_j^{fq} - \mu_j^{iq} N_j^{iq}) + (s^{fI} - s^{iI}) A^I \qquad [C3]$$

where superscripts i and f represent the initial and final state, respectively. Following the derivation of the nonequilibrium model,[1] the enthalpy change in the interface region can be written as:

$$\delta H^I = \delta H_*^I - \underline{H}_1^M \delta N_1^M - \sum_{j=2}^{n} \overline{H}_j^M \delta N_j^M \qquad [C4]$$

Since the enthalpy change in the interface region during interfacial segregation is equivalent to the interfacial cohesive energy change associated with interfacial segregation, the effect of interfacial segregation on the interfacial cohesive energy in continuous fiber metal matrix composite materials can be numerically estimated by using Eq. [C4].

Matrix (M)	
Interface (I)	s^I
Fiber (F)	
Interface (I)	s^I
Matrix (M)	

Fig. A1 — Model of the interface region in composite materials.

ACKNOWLEDGMENT

The authors would like to express their appreciation to the Air Force Office of Scientific Research for the partial support of this study under contract.

REFERENCES

1. J. P. Stark and H. L. Marcus: *Metall. Trans. A*, 1977, vol. 8A, pp. 1423-29.
2. M. Guttmann: *Surf. Sci.*, 1975, vol. 53, pp. 213-27.
3. J. Kameda and C. J. McMahon: *Metall. Trans. A*, 1980, vol. 11A, pp. 91-101.
4. J. Kameda and C. J. McMahon: *Metall. Trans. A*, 1981, vol. 12A, pp. 31-37.
5. L. Brewer: in *Electronic Structure and Alloy Chemistry of the Transition Elements*, P. A. Beck, ed., Interscience Publishers, 1963, pp. 221-35.
6. *Metals Handbook*, 8th edition, ASM, 1973, vol. 8.
7. R. A. Swalin: *Thermodynamics of Solids*, John Wiley & Sons, 1962.
8. H. L. Marcus, M. E. Fine, and L. H. Schwartz: *J. Appl. Phys.*, 1967, vol. 38, pp. 4750-58.
9. C. J. McMahon: *Mat. Sci. Eng.*, 1976, vol. 25, pp. 233-39.
10. B. J. Schulz and C. J. McMahon: in *Temper Embrittlement of Alloy Steels*, D. L. Newhouse, ed., ASTM STP 499, ASTM, 1972, pp. 91-103.
11. H. L. Marcus, L. H. Hackett, and P. W. Palmberg: in *Temper Embrittlement of Alloy Steels*, D. L. Newhouse, ed., ASTM STP 499, ASTM, 1972, pp. 91-103.
12. C. J. McMahon, A. K. Cianelli, and H. C. Feng: *Metall. Trans. A*, 1977, vol. 8A, pp. 1055-57.
13. H. Otani, H. C. Feng, and C. J. McMahon: *Metall. Trans.*, 1974, vol. 5, pp. 516-18.
14. H. Otani, H. C. Feng, and C. J. McMahon: *Metall. Trans. A*, 1976, vol. 7A, pp. 1123-31.
15. R. A. Mulford, C. J. McMahon, D. P. Pope, and H. C. Feng: *Metall. Trans. A*, 1976, vol. 7A, pp. 1183-95.
16. R. A. Mulford, C. J. McMahon, D. P. Pope, and H. C. Feng: *Metall. Trans. A*, 1976, vol. 7A, pp. 1269-74.
17. J. Yu and C. J. McMahon: *Metall. Trans. A*, 1980, vol. 11A, pp. 291-300.
18. P. R. Krahe and M. Guttmann: *Scripta Met.*, 1973, vol. 7, pp. 387-94.
19. M. Guttmann, P. R. Krahe, F. Abel, G. Amsel, M. Bruneaux, and C. Cohen: *Metall. Trans.*, 1974, vol. 5, pp. 167-77.
20. J. P. Coad, J. C. Riviere, M. Guttmann, and P. R. Krahe: *Acta Metall.*, 1977, vol. 25, pp. 161-71.
21. M. P. Seah: *Acta Metall.*, 1980, vol. 28, pp. 955-62.
22. R. J. Asaro: *Phil. Trans. R. Soc. Lond.*, 1980, vol. A295, pp. 151-63.
23. J. P. Hirth and J. R. Rice: *Metall. Trans. A*, 1980, vol. 11A, pp. 1501-11.
24. C. J. McMahon, V. Vitek, and F. R. Belton: *Scripta Met.*, 1978, vol. 12, pp. 785-89.
25. C. J. McMahon and V. Vitek: *Acta Metall.*, 1979, vol. 27, pp. 507-13.
26. W. Losch: *Acta Metall.*, 1979, vol. 27, pp. 567-73.
27. W. Losch: *ibid.*, pp. 1885-92.
28. C. L. Briant and R. P. Messmer: *Phil. Mag. B*, 1980, vol. 42, pp. 569-76.

29. R. P. Messmer and C. L. Briant: *Acta Metall.*, 1982, vol. 30, pp. 457-67.
30. C. L. Briant and R. P. Messmer: *ibid.*, pp. 1811-18.
31. M. Guttmann and D. McLean: in *Interfacial Segregation*, W. C. Johnson and J. M. Blakely, eds., ASM, 1979, pp. 251-348.
32. D. Y. Lee and H. L. Marcus: in *Metallurgical Treatises*, J. K. Tien and J. F. Elliott, eds., TMS-AIME, 1981, pp. 571-87.
33. J. R. Griffiths and D. R. J. Owen: *J. Mech. Phys. Solids*, 1971, vol. 19, pp. 419-31.
34. P. W. Palmberg, G. E. Riach, R. E. Weber, and N. C. MacDonald: *Handbook of Auger Electron Spectroscopy*, Physical Electronic Industries, 1976.
35. M. Schmerling, D. Finello, and H. L. Marcus: *Scripta Met.*, 1980, vol. 14, pp. 1135-38.
36. M. P. Seah: *Acta Metall.*, 1977, vol. 25, pp. 345-57.
37. P. L. Gruzin and V. V. Minal: *Phys. Met. Metallogr.*, 1963, vol. 16, pp. 551-56.
38. C. L. Briant: *Scripta Met.*, 1981, vol. 15, pp. 1013-18.
39. M. L. Jokl, V. Vitek, and C. J. McMahon: *Acta Metall.*, 1980, vol. 28, pp. 1479-88.
40. M. L. Jokl, J. Kameda, C. J. McMahon, and V. Vitek: *Met. Sci.*, 1980, vol. 14, pp. 375-84.
41. D. Y. Lee: Ph.D. Dissertation, The University of Texas at Austin, 1983.